PERGAMON

Vision Research 42 (2002) 3043–3058

Vision Research

www.elsevier.com/locate/visres

Computing heading in the presence of moving objects: a model that uses motion-opponent operators

Constance S. Royden *

Department of Mathematics and Computer Science, College of the Holy Cross, P.O. Box 116A, Worcester, MA 01610, USA

Received 18 January 2002; received in revised form 30 July 2002

Abstract

Psychophysical experiments have shown that human heading judgments can be biased by the presence of moving objects. Here we present a theoretical argument that motion differences can account for the direction of bias seen in humans. We further examine the responses of a computer simulation of a model for computing heading that uses motion-opponent operators similar to cells in the primate middle temporal visual area. When moving objects are present, this model shows similar biases to those seen with humans, suggesting that such a model may underlie human heading computations.

Keywords: Optic flow; Heading; Motion-opponent; Computational model; Middle temporal area

1. Introduction

When we move through the world, we often must judge our direction of motion (or heading) in the presence of moving objects. For example, when driving down a busy street we must be able to steer the car in the presence of other moving cars and pedestrians. People generally accomplish this task fairly easily. However, most models for computing heading rely on the assumption that the observer is moving through a stationary scene (Bruss & Horn, 1983; Cutting, Springer, Braren, & Johnson, 1992; Hatsopoulos & Warren, 1991; Heeger & Jepson, 1992; Lappe & Rauschecker, 1993; Longuet-Higgins & Prazdny, 1980; Perrone, 1992; Perrone & Stone, 1994; Rieger & Lawton, 1985; Royden, 1997). The presence of a moving object adds conflicting motion information to the scene. This conflicting information can cause biases in the heading computed by the model unless the object can be located and excluded from the computation. The presence of a moving object does not significantly affect human heading judgments under many conditions (Cutting, Vishton, & Braren, 1995; Royden & Hildreth, 1996; Warren & Saunders, 1995). However, under some conditions, human observers also show biases in heading judgments when a moving object is present (Royden & Hildreth, 1996; Warren & Saunders, 1995). It is therefore possible that a model developed with the assumption of a stationary scene would exhibit heading biases that are similar to the human biases seen in the presence of moving objects. These biases may provide some insight into the mechanisms used by the visual system for computing heading. Here, we examine the effect of moving objects on the performance of a heading model that is based on the motion-opponent properties of cells in the primate middle temporal visual area (MT). The results show how this model can explain some perplexing findings in the human psychophysical studies.

When an observer moves in a straight line, the retinal images of all points in the scene move in a radial pattern, as shown in Fig. 1(a). This motion of the images in the scene is known as the optic flow field. The center of this radial pattern, known as the focus of expansion (FOE), coincides with the observer's direction of motion (Gibson, 1950). Thus one can easily compute heading from such an optic flow pattern by finding the best intersection of lines through the image velocity vectors corresponding to the points in the flow field. Unfortunately, this approach fails when the observer undergoes a rotation, as when he or she moves along a curved path (Fig. 1(b)), or when there are moving objects in the scene (Fig. 1(c)). The rotation adds an extra component to the flow field that disrupts the radial pattern so that the

* Tel.: +1-508-793-2472; fax: +1-508-793-3530.

0042-6989/02/$ - see front matter
PII: S0042-6989(02)00394-2

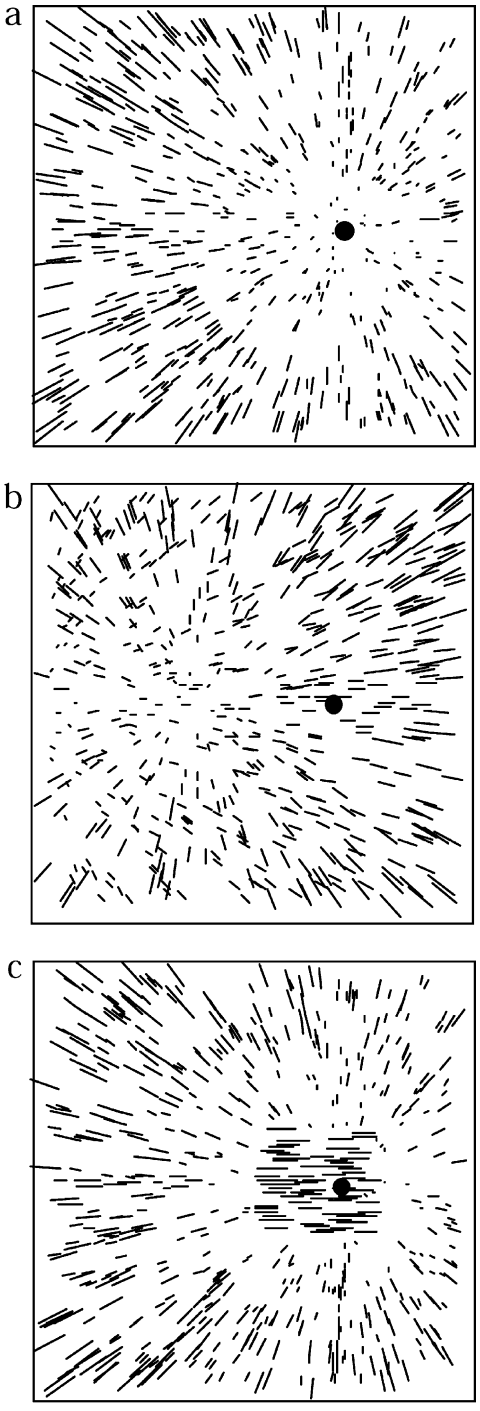

Fig. 1. Optic flow fields created by an observer moving toward two transparent frontoparallel planes of dots. Each line represents the image velocity of a single point in the scene. The direction of translation is indicated by a black circle in all three flow fields. (a) The flow field generated by an observer moving in a straight line toward a point 6 deg to the right of center. (b) The flow field generated by an observer with the same translation as in (a), but with an added rotation to the left about a vertical axis. (c) The flow field generated by an observer translating 6 deg to the right of center with an opaque object moving to the left in front of the two planes.

FOE no longer exists. The moving object adds velocity vectors that are inconsistent with the radial pattern, and thus can interfere with the calculation of heading. If the object moves in a straight line relative to the observer, it will have its own FOE. Thus a computation of the best intersection of lines through the velocity vectors would yield a point somewhere between the FOE for the stationary scene and the FOE for the moving object, as shown in Fig. 2. Consequently, one might expect that a moving object would cause a bias in heading judgments towards its own FOE. This is true of most template models for heading, i.e. those that use templates of radial patterns of flow to estimate heading (Hatsopoulos & Warren, 1991; Warren & Saunders, 1995). However, the psychophysical results show that humans only show this bias under some conditions, and in other conditions the biases do not conform to this prediction.

For motion in a straight line, recent psychophysical research has shown that under many conditions humans judge their heading accurately when a moving object is present (Royden & Hildreth, 1996; Warren & Saunders, 1995). However, when the object crosses the observer's path, it causes a small bias in heading judgments. The size and direction of this bias depends on the position and 3D direction of motion of the moving object. When the object moves toward the observer, humans show a bias in their heading judgments in the direction of the object's FOE (Royden & Hildreth, 1996; Warren & Saunders, 1995), consistent with the predictions from a template model as described above. However, when the object moves laterally with respect to the observer (i.e. the object maintains a constant distance from the ob-

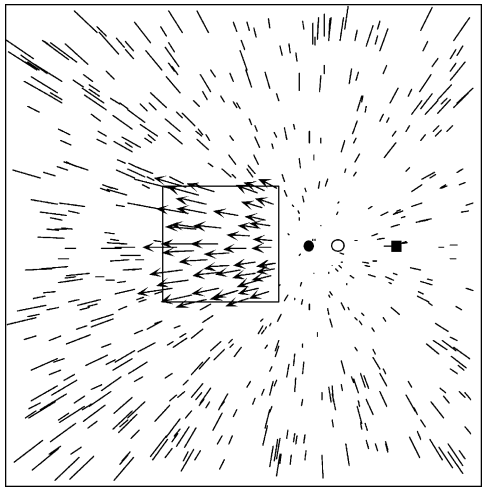

Fig. 2. Flow field generated from an observer's approach to two frontoparallel planes with a moving object in front. The object is outlined in the square. The image velocity vectors for the moving object are indicated by arrows and for the 2 transparent planes are indicated by line segments. The FOE for the stationary parts of the scene is shown with the black circle. The FOE for the object is shown by the black square. The open circle indicates the approximate expected heading estimate from a template model that uses velocity vectors as input.

server during each trial), Royden and Hildreth found that observers show a small bias (≈1 deg) in the direction of object motion. An object moving to the right causes a bias to the right, and a leftward moving object causes a leftward bias. This is the opposite of what one would expect from a template model which finds an average between the positions of the FOEs of the stationary and moving parts of the scene. The FOE of the moving object is in the direction opposite the lateral component of its 3D motion, so objects with a leftward component of motion would have an FOE to the right as shown in Fig. 2. Thus, a template model should show a bias to the right for a leftward moving object. This is the opposite of the direction of bias shown by humans.

At first glance the results from the psychophysics might seem contradictory. In the case of object motion in depth, the bias is opposite the object's lateral component of motion (and toward its FOE). In the case of pure lateral motion, however, the bias is in the same direction as the object's lateral component of motion (and opposite its FOE). Here we show that the direction of these biases can be explained if one considers a mechanism for computing heading that uses velocity differences instead of the velocity vectors themselves.

A model using difference vectors for computing heading was originally proposed by Longuet-Higgins and Prazdny (1980) as a way to compute heading in the presence of rotations. To understand how this model behaves in the presence of moving objects, it is useful to understand the theory underlying the original formulation of the model for dealing with rotations. Longuet-Higgins and Prazdny noted that when an observer is moving through the world, the image velocities in the flow field have two separate components, one which is due to the observer's translation (motion in a straight line) and one which is due to the observer's rotation. This can be seen from the following derivation. Consider a point P in a scene at a position (X, Y, Z). The image position, p, of that point on an image plane at focal distance of 1 unit from the center of projection is given by $p = (x, y) = (X/Z, Y/Z)$. For an observer moving through a scene with a translational velocity (T_x, T_y, T_z) and rotational velocity given by (R_x, R_y, R_z), the image velocity of point p is given by the following equations:

$$v_x = (-T_x + xT_z)/Z + R_x xy - R_y(x^2 + 1) + R_z y,$$
$$v_y = (-T_y + yT_z)/Z + R_x(y^2 + 1) - R_y xy - R_z x,$$

where v_x is the horizontal component of the image velocity and v_y is the vertical component. These equations are each separable into a component that depends only on observer translation (t_x, t_y) and a component that depends only on observer rotation (r_x, r_y).

$$t_x = (-T_x + xT_z)/Z,$$
$$t_y = (-T_y + yT_z)/Z,$$

$$r_x = R_x xy - R_y(x^2 + 1) + R_z y,$$
$$r_y = R_x(y^2 + 1) - R_y xy - R_z x,$$

The magnitude of the translation component depends on depth, Z, while the rotation component is independent of depth. Thus, if one has two points at different distances along a line of sight, for example at the border between two surfaces that are at different distances from the observer, subtracting the image velocity of one from the image velocity of the other will eliminate the rotation components and leave a "difference vector" that depends only on observer translation. The difference vector is given by:

$$v_{xd} = (-T_x + xT_z)(1/Z_1 - 1/Z_2),$$
$$v_{yd} = (-T_y + yT_z)(1/Z_1 - 1/Z_2),$$

where v_{xd} is the horizontal component and v_{yd} is the vertical component of the difference vector and Z_1 and Z_2 are the distances from the two different surfaces.

Longuet-Higgins and Prazdny further showed that these difference vectors point directly toward or away from the observer's translational heading direction. Thus, by performing this vector subtraction between image velocities for adjacent points throughout the entire optic flow field, one can eliminate the rotation component of flow. One can then find the direction of translation by finding the intersection of lines through the resulting difference vectors, which will be non-zero at the locations of depth discontinuities.

This model was extended by Rieger and Lawton (1985), who showed that the subtraction could be performed for points that were separated slightly on the image plane. Hildreth (1992) created a version of this model that located a heading that was consistent with velocity difference information from the majority of the regions in the scene, thus eliminating the effect of small moving objects. Hildreth (1992) pointed out that one could also use such a model to locate the image velocities due to moving objects, since those objects would generate difference vectors that were inconsistent with the radial pattern of the difference vectors associated with stationary parts of the scene. Finally, Royden (1997) showed that spatially extended motion-opponent operators that were designed based on the receptive field properties of neurons in the primate visual area MT could accomplish this motion subtraction well enough to compute the translational heading direction in the presence of rotations. It should be noted that, while these models were developed to compute heading in the presence of rotations, they also function well in the absence of rotations, provided there is some depth variation in the scene.

When there are moving objects in the scene, difference vectors generated at the borders of the moving object have directions that differ from the radial pattern of the

difference vectors associated with the stationary part of the scene. If these difference vectors are included in the computation of heading, one would expect them to cause biases in the heading estimate related to the angle of the vectors. Thus, analyzing the directions of these vectors should lead to insight as to how models based on motion differences should be affected by moving objects.

Fig. 3(a) shows the difference vectors generated at the borders of an object moving horizontally to the left for the conditions used in Experiment 1 of Royden and Hildreth (1996). In this case lines through the vectors appear to intersect at a point to the left of the object, i.e. in the direction of object motion. This direction is consistent with the leftward bias shown by human observers. Fig. 3(b) shows the difference vectors generated at the borders of an object moving in depth whose FOE is to the right of the observer's heading (i.e. its lateral component of motion is to the left). These difference vectors appear to intersect at a point to the right of the observer's heading, consistent with the rightward bias shown by human observers. In fact, the difference vectors at the borders of a moving object can be shown to intersect at a single point that depends on the motion of the observer and the motion of the object. The difference vectors are given by the following equations:

$$v_{xd} = (-T_{x1} + xT_{z1})/Z_1 - (-T_{x2} + xT_{z2})/Z_2,$$
$$v_{yd} = (-T_{y1} + yT_{z1})/Z_1 - (-T_{y2} + yT_{z2})/Z_2,$$

where the observer motion relative to the stationary scene at distance Z_1 is (T_{x1}, T_{y1}, T_{z1}) and the observer motion relative to the moving object at distance Z_2 is (T_{x2}, T_{y2}, T_{z2}). The point of intersection of lines through these vectors is given as:

$$x = (Z_2T_{x1} - Z_1T_{x2})/(Z_2T_{z1} - Z_1T_{z2}),$$
$$y = (Z_2T_{y1} - Z_1T_{y2})/(Z_2T_{z1} - Z_1T_{z2}).$$

Table 1 shows the intersection point for the difference vectors at the borders of the moving objects used in the experiments of Royden and Hildreth (1996). In these experiments, each trial simulated observer motion toward two transparent frontoparallel planes of dots, at initial distances of 400 and 1000 cm from the observer. The simulated observer speed was 200 cm/s toward a position 6 deg to the right of center. The top two rows of the table show the calculated intersections of difference vectors for an object moving laterally with respect to the observer with a speed of 8.1 deg/s to the left or right. The bottom two rows show the calculated intersections for an object moving toward the observer with a speed of 300 cm/s and with an FOE at 1 deg or 10 deg to the right of center. For the laterally moving objects (Experiment 1 from Royden and Hildreth), the vectors intersect at a point that is shifted in the direction of motion of the object relative to the observer heading. For the objects moving in depth (Experiment 8 in Royden and Hildreth), the vectors intersect at a point that is shifted in the direction of the object's FOE. Thus, if all the difference vectors in the scene were used to compute the observer's heading, the difference vectors at the borders of the moving object should cause a bias that is consistent with that seen for human observers. To determine whether a physiological version of this difference vector model would exhibit these same tendencies, we tested the Royden (1997) model for its ability to compute heading in the presence of moving objects.

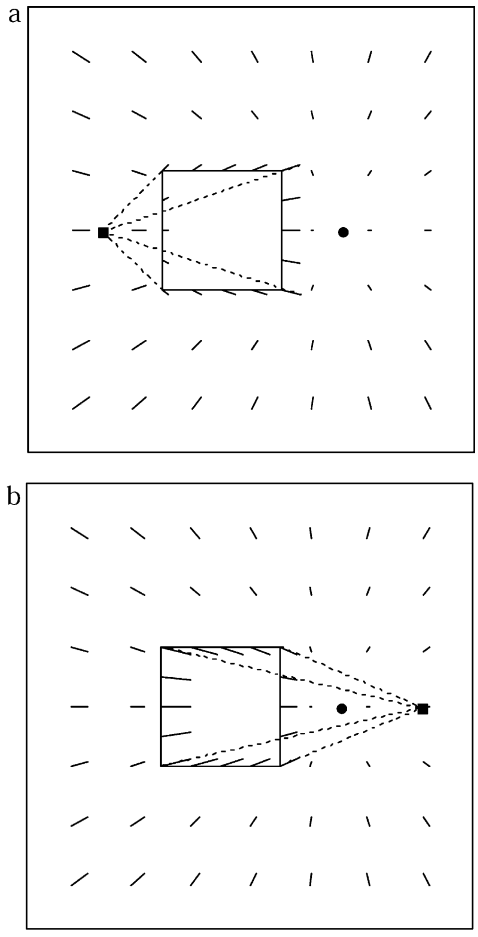

Fig. 3. Difference vectors for flow fields containing moving objects. (a) Difference vectors for approach toward two frontoparallel planes with an object moving laterally to the left with no component of motion in depth. Note that the lines through the difference vectors at the border of the object intersect at a point (indicated by the black square) to the left of the translational direction (indicated by the black circle). (b) Difference vectors for approach toward two frontoparallel planes with an object moving in depth toward the observer, with an FOE at 10 deg to the right of center. This FOE is to the right of the observer's heading, which is located at 6 deg to the right of center. The horizontal component of motion for this object is to the left. Note that the dotted lines extending through the difference vectors at the border of the object intersect at a point (indicated by the black square) to the right of the translational heading (indicated by the black circle).

Table 1

Object direction	Simulated heading (deg)	Time (s)	Intersection (deg) near plane	Intersection (deg) far plane
Left	6.0	0.0	−10.1	−31.0
		0.8	−3.7	−26.0
Right	6.0	0.0	21.2	39.1
		0.8	15.4	35.0
1 deg FOE	6.0	0.0	−8.8	−0.8
		0.8	−2.9	−0.3
10 deg FOE	6.0	0.0	17.9	11.45
		0.8	13.3	10.6

Table showing the intersection of the difference vectors generated at the borders of moving objects for the conditions used in Royden and Hildreth (1996) and in the current study. Observer speed was 200 cm/s toward a position located at 6.0 deg to the right of center. The stationary scene consisted of 2 planes located at 400 and 1000 cm from the observer at the beginning of the trial. For the laterally moving object the motion was left or right with a speed of 8.1 deg/s at a distance of 400 cm from the observer. For the object motion in depth, the object's speed was 300 cm/s with an FOE of 1 deg or 10 deg to the right of center. The initial distance of the object was 400 cm from the observer. Intersection points are given for the difference vectors generated from the object and the near plane and for the difference vectors generated from the object and the far plane, for the beginning ($t = 0$ s) and end ($t = 0.8$ s) of the trial. Negative numbers indicate positions to the left of center.

2. The computational model

The computational model (described in more detail in Royden (1997)) is based on the receptive field properties of neurons in area MT of the primate visual system. These cells have receptive fields with excitatory centers that are tuned to direction and speed of moving stimuli (Maunsell & van Essen, 1983). Thus they respond best to a visual stimulus within their receptive field that moves in a preferred direction of motion and their response decreases as the direction of motion deviates from this preferred direction. The cells are similarly tuned to the speed of the stimuli. In addition to the excitatory center, many of these cells exhibit an inhibitory "surround". Motion in this region, contiguous with the center region, inhibits the response of the cells to motion in the center (Allman, Miezin, & McGuiness, 1985; Raiguel, Van Hulle, Xiao, Marcar, & Orban, 1995). For the majority of these cells, the inhibition is maximum when the direction of motion in the inhibitory region is in the preferred direction of motion of the excitatory region. Thus these cells respond poorly to uniform motion that covers both the excitatory and inhibitory regions of their receptive fields, and respond best when there is a difference in motion across the boundary between the center and surround. The spatial arrangement of the excitatory and inhibitory regions varies from cell to cell, with some exhibiting a center-surround structure and others exhibiting more asymmetric arrangements, with the inhibitory region on one side of the excitatory region (Xiao, Raiguel, Marcar, Koenderink, & Orban, 1995).

The model uses a simplified implementation of these cells, shown in Fig. 4(a). Each operator in the model (referred to from here on as "motion-opponent operators") has a receptive field in which one half is excitatory and the other half inhibitory. Both the excitatory and inhibitory sides are tuned to the same direction of

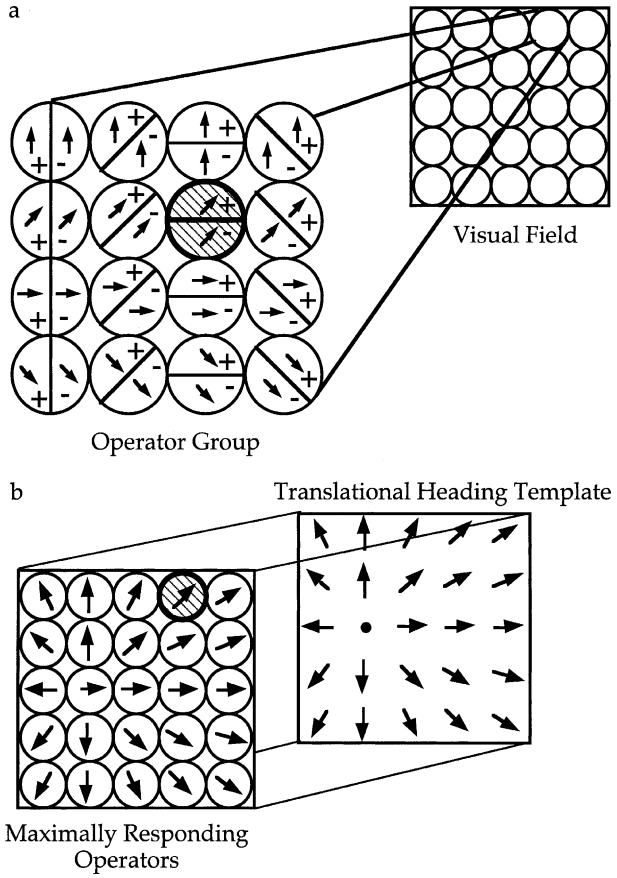

Fig. 4. Computational model for computing heading. (a) Each region of the visual field is processed by a group of motion-opponent operators that differ in their preferred direction of motion and the angle of the axis between the excitatory and inhibitory regions. Arrows indicate the preferred direction of motion. The diagonal fill lines indicate an operator with a hypothetical maximum response. (b) The maximally responding operator of each group, indicated by the diagonal line fill, contributes to the responses of cells in the template layer if their preferred direction of motion matches the radial pattern of the template. Each template cell is tuned to a radial pattern with a specific location of the center. The center of the maximally responding template cell corresponds to the observer's translational direction of motion.

motion, and the response of the operator is computed as the response of the excitatory region minus the response of the inhibitory region. The response of each region of the receptive field is computed by finding the average velocity of visual features (dots in the simulation) that fall within that region and multiplying by the cosine of the angle between this average direction and the preferred direction of motion of the cell.

The motion-opponent operators are organized as shown in Fig. 4(a). Each region of the visual field is processed by a group of operators that have the same receptive field position but vary in their preferred direction of motion and in the angle of the axis between the excitatory and inhibitory regions. For a given visual input, the operator within this group that has the greatest response has a preferred direction that points approximately toward the point in the image that corresponds to the observer's translational direction of motion. These maximally responding operators then project to another layer of operators (Fig. 4(b)). This second layer consists of operators that have large receptive fields that are templates for radial patterns of difference vectors. Each operator has a different preferred center of expansion for this radial pattern, corresponding to a preferred direction of translation of the observer. The operator that responds most strongly in this second layer indicates the direction of translation of the observer. The operators in this second layer have properties similar to some of the neurons found in the primate medial superior temporal visual area (MST). This area, which is thought to be involved in heading computation, receives input from area MT and has cells which respond to expanding or contracting motion within their receptive fields (Duffy & Wurtz, 1991; Graziano, Andersen, & Snowden, 1994; Saito et al., 1986; Tanaka & Saito, 1989) as would the template cells in the model. The mean square root of the area of the receptive fields of these cells is large, on the order of 40 deg, similar to the size of the template cells in the model (Tanaka & Saito, 1989). Also, many of the cells in MST are tuned to different positions of the center of expansion (Duffy & Wurtz, 1995), which is another feature of the model's template cells. Thus the model's two layers are similar to areas MT and MST of the primate visual system.

This model computes translational heading well for simulations of motion through stationary scenes. It consistently computes translational heading well in the presence of simulated observer motions containing both translation and rotation. It is fairly robust in the presence of noise added to the image velocity vectors (see Royden, 1997 for a more thorough analysis of the model). The goal in the current set of studies is to examine this model's behavior in the presence of moving objects. Because of its reliance on motion differences, one might expect this model to exhibit biases similar to those seen with human subjects, because the difference vectors along the borders of the objects point in the direction of these biases.

3. The model simulations

Simulations were run using the model described above and scenes that were similar to those used in Royden and Hildreth (1996). The parameters of the model were similar to those used to generate good model performance in the presence of rotations (Royden, 1997). However, it should be noted that the model's response is fairly robust to changes in these parameters. Changing receptive field size by ± 1 deg, varying the tuning width over a fairly broad range or decreasing the number of preferred directions had little effect on the model responses (Royden, 1997). In the current study, the radius of each operator's receptive field was 2 deg, and the spacing of the receptive fields was 2 deg. Thus there was an overlap between adjacent operators. Each receptive field region was analyzed by 192 operators, representing 24 different preferred directions of motion (equally spaced between 0 and 360 deg) and eight different angles of the axis between the excitatory and inhibitory regions (evenly spaced between 0 and 180 deg). As described above, the response of each operator was computed as the response magnitude from the excitatory region minus the response magnitude in the inhibitory region. The response magnitude for each region was computed as the product of the speed of the average velocity within the region and the cosine of the angle between the direction of the average velocity and the preferred direction of the operator. This response is described in the following equation:

$$R_{\mathrm{op}} = v_{\mathrm{avg}+}\cos(\theta - \phi_{+}) - v_{\mathrm{avg}-}\cos(\theta - \phi_{-})$$

where θ is the preferred direction of the operator, $v_{\mathrm{avg}+}$ and ϕ_{+} are the speed and direction of the average motion in the excitatory part of the operator's receptive field, and $v_{\mathrm{avg}-}$ and ϕ_{-} are the speed and direction of the average motion in the inhibitory part of the operator's receptive field.

The response of each of the template cells was computed as follows. Each template cell had a receptive field covering the entire field of view for the simulation (30×30 deg). The centers of the radial patterns (i.e. the preferred heading direction) of the template cells were evenly spaced every 2 deg both horizontally and vertically between -12 and $+12$ deg. Thus there were 169 total template cells. For each region of the visual field, the maximally responding motion-opponent operator projected to the template layer. For each template cell, a motion-opponent operator contributed to its response if the preferred direction of that operator pointed toward

or away from the preferred radial center of the template cell, within a margin of error determined by the spacing between preferred centers. The motion-opponent operator contributed an amount equal to its magnitude of response weighted by a Gaussian function of the distance between the motion-opponent operator's receptive field and the center of expansion of the template cell. Thus motion-opponent operators with receptive fields close to the center of expansion contributed more strongly to the template cell's response than those that are further away. The response can be described in the following equation:

$$R_{\text{template}} = \Sigma_{(\text{input cells})} R_{\text{op}} e^{-(d^2/2\sigma^2)}$$

where R_{op} is the response of each motion-opponent operator and d is the distance between the center of the input operator and the center of the preferred radial pattern of the template cell. In each of the simulations run here, σ is constant at 10.0 deg. The summation is over each of the maximally responding operators within the input field of the template cell.

The inputs to the model were computed based on the simulated scenes below. The 3D positions of individual points were randomly generated to lie on a given surface. The 2D image positions and velocities of these points were computed based on the 3D position of the point, and the observer's motion relative to that part of the scene. These 2D image velocities were then used as inputs to the model simulations. Simulations were run multiple times (usually 50) with different random positioning of points in each trial.

4. Simulation 1: heading with a laterally moving object

4.1. Conditions

This simulation replicated the conditions used in Experiment 1 of Royden and Hildreth (1996), in which subjects viewed a simulated scene of an observer moving toward two transparent planes of moving dots that had an independently moving object in front of them. The object moved laterally with respect to the observer, i.e. it did not change depth during the trial. The two planes, consisting of 500 dots, were at initial positions of 400 and 1000 cm from the observer and the observer's speed relative to the planes was 200 cm/s. The simulated

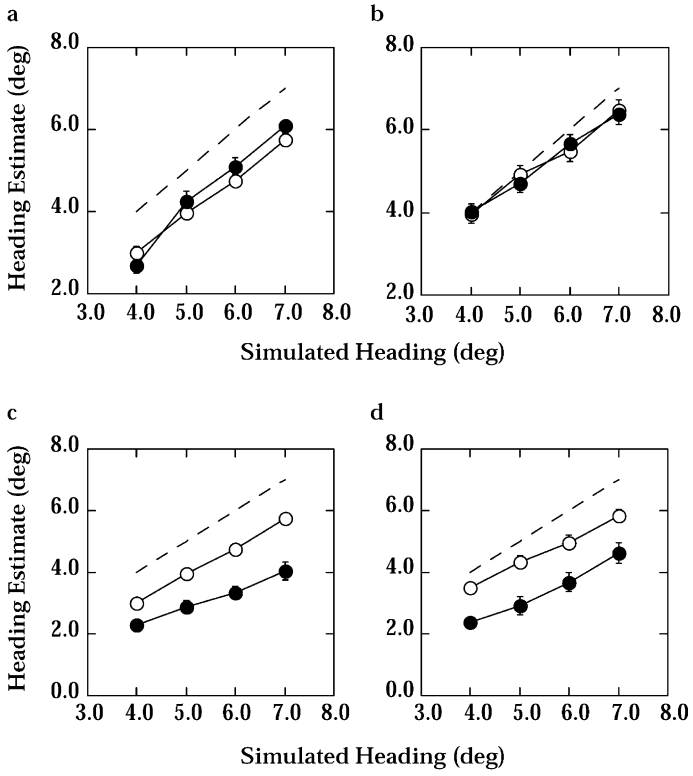

Fig. 5. Data from the model and from psychophysics for a laterally moving object. Each graph shows the average heading estimate given by the model (a and c) or a human subject (b and d). Open symbols indicate the condition for which no moving object was present. Filled symbols indicate the response when a leftward moving object was present. Simulated headings were 4, 5, 6 or 7 deg to the right of center. Graphs (a) and (b) show the responses for the case where the object starting position is located at −1.4 deg (i.e. 1.4 deg to the left of center). Graphs (c) and (d) show the responses for the case when the object starting position is located at 10.7 deg to the right of center. Error bars indicate 1 standard error (SE) above and below each data point. (Points with no visible error bars have a SE that is smaller than the plot symbol in the graph.)

headings were 4, 5, 6 or 7 deg to the right of the center of the screen. The object was a 10×10 deg square consisting of 80 points. It moved to the left or right at a speed of 8.1 deg/s. For a left moving object, object positions of −1.4, 0.6, 4.7, 8.7, 10.7 and 12.7 deg were tested. For the right moving object, positions of −9.9, −5.9, −1.9, 0.2, 2.2 and 6.3 deg were tested, as in the psychophysical experiments. In addition, one condition with no moving object present was also tested. The viewing window was 30×30 deg. For each simulation run, the model program generated a set of points randomly positioned in the scene—500 points on the stationary planes and 80 points on the moving object. An image position and image velocity was then computed for each point in the scene. These positions and velocities were then used as input for the model. The model was tested for each of the 4 headings and for each of the 6 object positions plus the condition with no object present. Each condition was run 50 times. The data presented below show the average over the 50 trials.

4.2. Results

Fig. 5 shows the heading estimates of the model for the case with no moving object and for the case where there is a moving object present. In Fig. 5(a), the moving object's center is positioned at 1.4 deg to the left of the center of the visual field. In this condition, there is little effect of the moving object on the model's heading estimates. The same was found for human observers in this condition, as can be seen from the human data from Royden and Hildreth (1996), re-plotted in Fig. 5(b). The model shows a slightly larger bias toward the center of the scene than this particular subject, even in the condition with no object present in the scene. This central bias is often seen with humans (Cutting et al., 1992; Royden & Hildreth, 1996) and the model's bias is within the range seen for humans. For example, notice the central bias shown by the subject in Fig. 5(d). Fig. 5(c) shows the model estimates for the condition with the moving object positioned at 10.7 deg to the right of center. In this case for each heading there is a substantial bias to the left caused by the presence of the moving object. This is similar to the bias seen in human observers in Royden and Hildreth, as shown for one observer in Fig. 5(d).

Fig. 6 compares the average bias generated by the model with that seen for human observers. The graph shows the average bias caused by the presence of a moving object in the scene, i.e. the difference in the heading estimate when the object is present and when the object is absent, with respect to the object's position in the scene. The biases for the 4 different headings have been averaged together in these graphs. It is clear from this figure that the model shows a bias in the same direction and of a similar magnitude to that of human observers. For a leftward moving object, the average bias for the model had a maximum of 1.26 deg to the left, while the average bias for humans had a maximum of 0.94 deg to the left. For the rightward moving object the maximum average bias was 0.78 deg to the right, compared to 0.56 deg to the right for the humans. In both cases, the position of the object affected the size of the bias. When the object covered the FOE of the stationary scene, the effect was largest. This is due in part to the Gaussian weighting of the input to the template cells, with operators closer to the FOE having a larger weight. The model produced very consistent results for these conditions, with repeated runs of the simulation generating the same direction and similar magnitudes of bias.

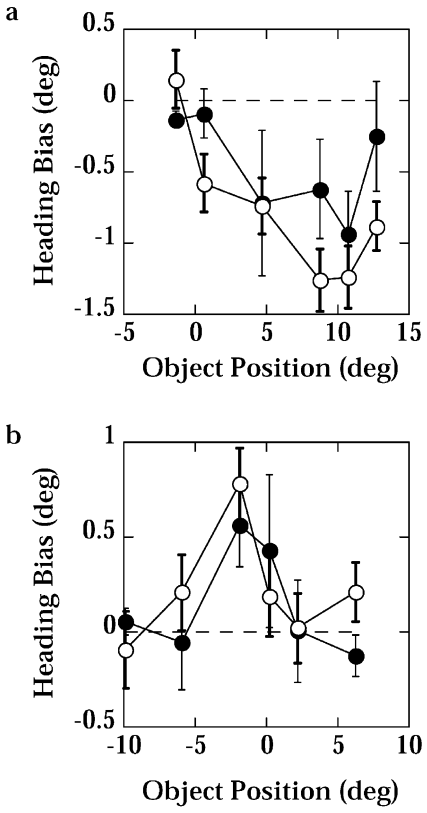

Fig. 6. Biases in heading estimates caused by a laterally moving object starting at different positions. Each graph plots the heading bias caused by the presence of a moving object, i.e. the difference in the heading estimate for the condition when the object is present and the estimate when the object is absent. A positive bias indicates a bias to the right, while a negative bias indicates bias to the left. The object positions indicate the starting position of the object in degrees. Negative numbers indicate starting positions to the left of center and positive numbers are to the right of center. Open symbols indicate the average response of the model and filled symbols indicate the average response of human observers (re-plotted from Royden & Hildreth, 1996). Error bars represent 1 SE above and below each data point. Error bars for the model results are shown with slightly thicker lines than those for the human results. (a) Data for a leftward moving object. (b) Data for a rightward moving object.

5. Simulation 2: heading with an object moving in depth

5.1. Conditions

This simulation used conditions similar to those in Royden and Hildreth Experiment 8, in which an object moved in depth relative to the observer. The stationary scene and the observer motion toward the scene were the same as in the first simulation, with the observer moving toward two transparent planes of dots with a speed of 200 cm/s. The moving object consisted of an opaque square of dots that moved toward the observer with a speed of 300 cm/s and an angle of motion relative to the observer of either 1 or 10 deg to the right of the center of the viewing window. The 1 deg direction of object motion was to the left of all simulated headings and the 10 deg direction of motion was to the right of all simulated headings. Object starting positions of 0.6, 2.25, 3.9, 5.5 and 7.1 deg were tested for both object motion directions. In addition, a starting position of −1.0 deg was tested for the object with a 1 deg FOE, and a starting position of 9.9 deg was tested for the object with a 10 deg FOE. The object's starting size was 8×8 deg. Because the layout of the scene changes considerably over time, with the object growing in size over the course of the trial as it approaches the observer, heading estimates were simulated for times of 0, 0.4 and 0.8 s into the trial. (The trials in the psychophysical experiments were 0.8 s long.) Each condition was run 50 times and the average heading estimate over these 50 trials is presented here.

5.2. Results

Fig. 7 shows the average bias generated by the model with respect to the starting position of the moving object for $t = 0$ (Fig. 7(a) and (b)) and 0.4 s (Fig. 7(c) and (d)). As predicted by the difference vector analysis above, the model shows a leftward bias for the moving object with a 1 deg FOE (to the left of the simulated headings) and a rightward bias for the moving object with a 10 deg FOE (to the right of the simulated heading). The bias increases with increasing time, with the biases for $t = 0.8$ s reaching a maximum of 5.5 deg. This is not surprising, since the object's image size grows from 8×8 deg at the beginning of the trial to about 19×19 deg at the end of the trial. Thus, there is much more information for heading computation along the

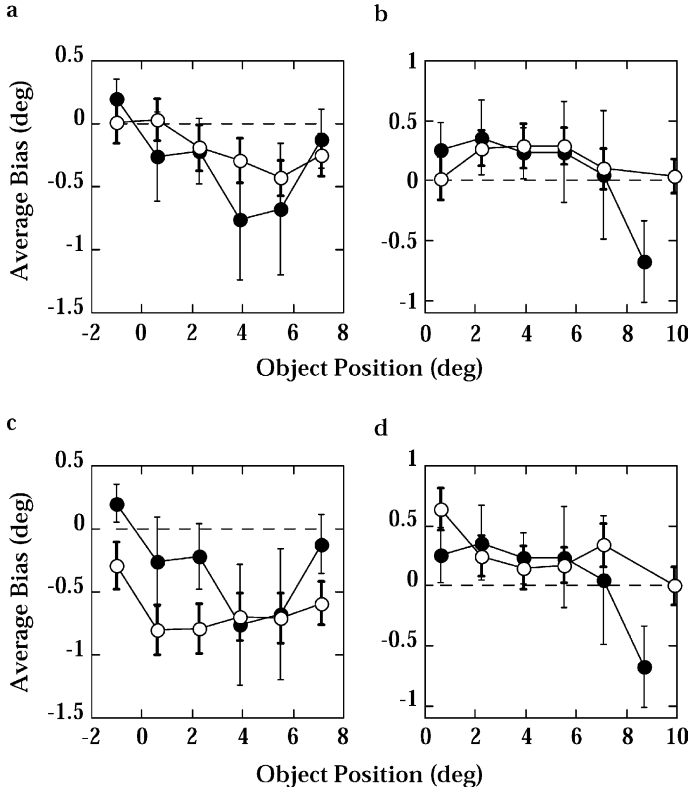

Fig. 7. Biases in heading estimates caused by an object moving in depth for an object starting at different positions. Graphs (a) and (b) show bias for time $t = 0$ s. Graphs (c) and (d) show bias for time $t = 0.4$ s. Open circles show the average response of the model. Filled circles indicate average data for human observers (re-plotted from Royden & Hildreth, 1996). Error bars indicate 1 SE above and below each point. Thicker error bars are used for the model results. Graphs (a) and (c) show data for an object with FOE at 1 deg to the right of center (and therefore to the left of the simulated headings). Graphs (b) and (d) show data for an object with FOE at 10 deg to the right of center (and therefore to the right of the simulated headings).

borders of the object at 0.8 s than there is at the beginning of the trial. This will lead to more influence of the object on heading judgments at the later times. The results of the human psychophysics (Royden & Hildreth, 1996 , Experiment 8) are also re-plotted on the graphs in Fig. 7. The biases seen in humans fall somewhat in between the biases generated by the model at $t = 0$ and 0.4 s. Fig. 8 plots the human data against the average of the model responses at $t = 0$ and 0.4 s. The results of these two are quite similar. The maximum leftward bias for the object with a 1 deg FOE was 0.76 deg to the left for the human data and 0.57 deg to the left for the model data averaged between 0 and 0.4 s. For the object with the 10 deg FOE, the bias for humans was 0.36 deg to the right and for the model was 0.33 deg to the right. The overall shapes of the curves are also similar. The only major difference between the simulations and the human data is the leftward bias seen with human judgments for the rightmost object position for the object with the 10 deg FOE. The model did not exhibit this leftward bias.

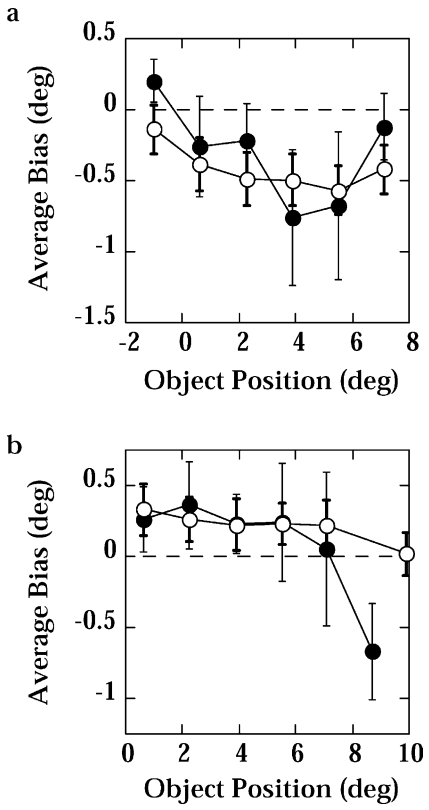

Fig. 8. Average bias for times $t = 0$ and 0.4 s for an object moving in depth. Open circles indicate the average bias for the model from times $t = 0$ and 0.4. Filled circles indicate the human data re-plotted from Royden and Hildreth (1996). Error bars for the model represent the average SE for times 0 and 0.4 s for each point. Error bars for the human data represent 1 SE above and below each point, as before. (a) Data for an object with FOE at 1 deg to the right of center. (b) Data for an object with FOE at 10 deg to the right of center.

6. Simulation 3: center-surround operators

6.1. Conditions

In this simulation we sought to test the effects of other spatial structures in the receptive fields of the motion-opponent operators in MT. As stated above, the excitatory and inhibitory regions of the motion-opponent cells in MT can have several different spatial arrangements. These include the asymmetric arrangement used in the above simulations as well as a center-surround organization, in which the inhibitory region surrounds the excitatory region (Xiao et al., 1995). Royden (1997) showed that the center-surround operators also are capable of determining heading in the presence of rotations, but they are less sensitive to gradual depth changes, such as those that occur with slanted planes. Given that these operators also compute motion differences, one would expect them to exhibit biases in the same direction as the asymmetric operators. We tested this by modifying the model to use center-surround operators instead of asymmetric operators. Each operator consisted of a central excitatory region, with radius 1.414 deg, with an outer inhibitory annulus with outer radius 2.0 deg. Each receptive field region was analyzed by 24 operators, representing 24 different preferred directions of motion, equally spaced between 0 and 360 deg. Because of the circular symmetry of the operators, it was unnecessary to have different operators representing the different angles of the axis between the excitatory and inhibitory regions. The receptive fields of each group of operators were spaced every 2 deg as with the asymmetric operators. The responses of the operators and the heading templates were computed as before. Simulations were run for the same conditions as for the previous two simulations. Simulations were run for times of 0, 0.2 and 0.4 s for the left and right moving object and 0 and 0.4 s for the looming objects. Each condition was run 50 times and the average heading estimate for the 50 trials is presented here.

6.2. Results

The results for the center-surround operators were similar to those found with the asymmetric operators. Fig. 9(a) and (b) show the results for the left and right moving objects for time $t = 0.2$ s. Responses at the other times were similar both in the shape and magnitude of the response. The response for the left moving object is a similar shape to that of the asymmetric operators, but the bias is somewhat decreased, with a maximum of 1.04 deg, which is slightly less than the asymmetric maximum of 1.26 deg and slightly greater than the human average maximum of 0.94 deg. The response for the right moving object shows two peaks, one slightly to the left of the human and asymmetric peaks and one slightly to the

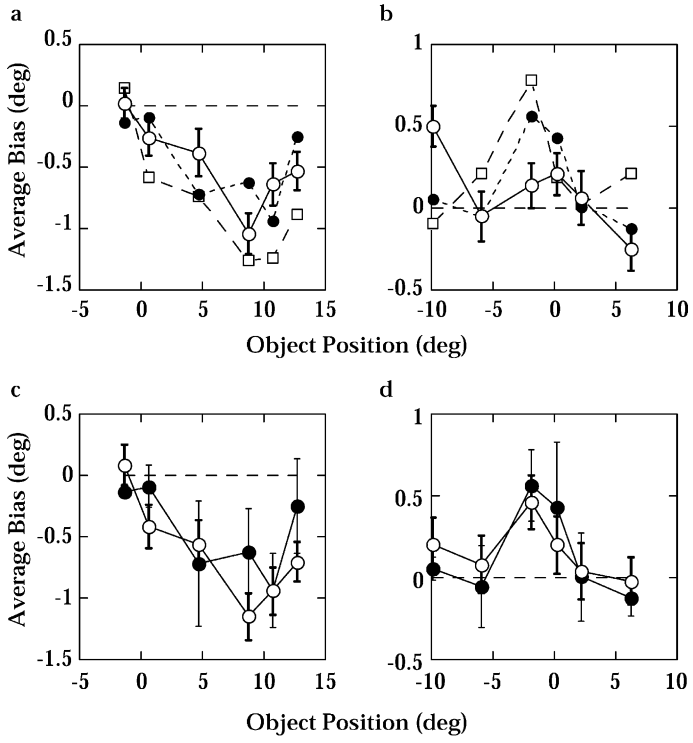

Fig. 9. Biases in heading estimates caused by a laterally moving object for a model using center-surround operators. (a) Responses of the model using center-surround operators (open circles) for a leftward moving object. Error bars indicate 1 SE above and below each point. Responses using asymmetric operators (open squares) and human responses (filled circles) are re-plotted from Fig. 6 for comparison. (b) Responses for a rightward moving object. All symbols are as in graph (a). (c) Average of center-surround and asymmetric operator responses (open circles) compared to average response of humans (filled circles) for a leftward moving object. Error bars for the model responses are the average SE for the center-surround and asymmetric cases. Error bars for the human data are 1 SE above and below each point. (d) Average of center-surround and asymmetric operator responses for a rightward moving object. All symbols are as in graph (c).

right of these peaks. This dual peak could be due to the spatial structure of the center-surround operators, which compute the differences at two horizontal locations, one on either side of the center. The maximum bias for the rightward moving object was 0.5 deg, slightly less than the maximum response of 0.78 deg for the asymmetric operators and 0.56 deg for the human data. The average response for the asymmetric and center-surround operators, shown in Fig. 9(c) and (d), is very similar to the human responses.

Fig. 10 shows the results for simulations using an object moving in depth with an FOE of 1 deg or 10 deg to the right of center. The average response between times of 0 and 0.4 s is shown. The response of the model using center-surround operators is similar to that of the asymmetric operators except that the response is shifted to the left, toward the center of the viewing window, by a small amount. This results in a slightly larger leftward bias (a maximum shift of 0.29 deg) when the moving object has an FOE at 1 deg, while the rightward bias is diminished for the moving object with the FOE at 10 deg (a maximum shift of 0.32 deg). This shift results in a slight leftward bias for some of the object positions for the object with the 10 deg FOE, something also seen with the human results. The average biases between the asymmetric and center-surround simulations are of similar magnitude to those seen with humans, as shown in Fig. 10(c) and (d).

7. Discussion

The data presented here show that a model based on the motion-opponent properties of the receptive fields of cells in primate visual area MT gives very similar heading results to those seen with human observers in the presence of moving objects. This is consistent with what might be expected for a model that makes use of motion differences to compute heading, since these motion differences lead to difference vectors at the borders of the moving objects that point in the direction of the observed bias. It is interesting to note that very little was added to the original model for computing heading in stationary scenes in order to achieve this result with moving objects. The only change was to add a Gaussian weighting to the connections between the motion-opponent operators in the first layer and the template cells in the second layer of the model. It was not necessary to

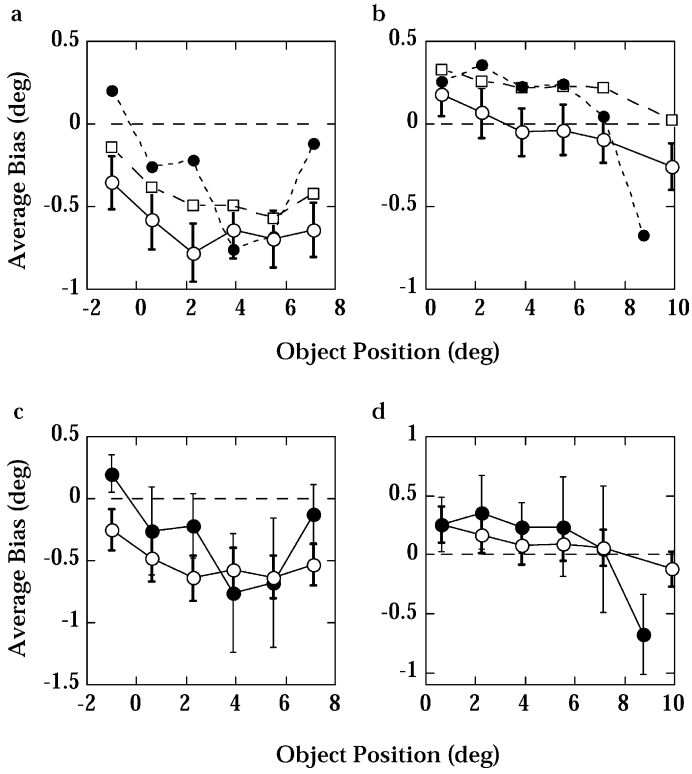

Fig. 10. Biases in heading estimates caused by an object moving in depth for a model using center-surround motion-opponent operators. (a) Average of responses at $t = 0$ and 0.4 s of model using center-surround operators (open circles) for a moving object with FOE at 1 deg to the right of center. Error bars indicate the average SE for the $t = 0$ and 0.4 conditions. Responses using asymmetric operators (open squares) and human responses (filled circles) are re-plotted from Fig. 8 for comparison. (b) Average of responses at $t = 0$ and 0.4 s for an object with an FOE at 10 deg to the right of center. All symbols are as in graph (a). (c) Average of center-surround and asymmetric operator responses (open circles) compared to average response of humans (filled circles) for a moving object with FOE at 1 deg to the right of center. Error bars for the model responses are the average SE for the center-surround and asymmetric cases. Error bars for the human data is 1 SE above and below each data point. (d) Average of center-surround operators and asymmetric operator responses for a moving object with FOE at 10 deg to the right of center. All symbols are as in graph (c).

locate the moving object and remove it from the computation of heading, as suggested in other models, such as Hildreth (1992). Instead, the similarity between the human and model results suggest that there need be no special mechanism to handle moving objects when computing heading. One can speculate that this is because the effects of the objects are small and only occur in special circumstances, when the object crosses the observer's path. Since the objects are moving, in most cases these conditions would only last a limited period of time. Thus there is no compelling reason to develop a separate mechanism to remove their effects.

7.1. Gaussian tuning of templates

As mentioned above, the one modification to the original model was to apply a Gaussian weighting to the inputs of the template layer. This weighting is only necessary to give the model the same position effect as seen with human observers. The Gaussian weighting causes the moving objects to have no effect on heading estimates when the objects are away from the FOE of the true heading (i.e. they are not crossing the observer's path). When it is not included, the model shows biases for all moving object positions. Warren and Saunders (1995) also added a Gaussian weighting to their template model to account for this position effect. It should be noted that this is not the only way one can achieve this result. For example, refining the heading estimate over time by increasing weight to motion inputs near the current heading estimate and decreasing weights from inputs further away, as suggested by Royden and Hildreth (1996), also accomplishes the same result. This can be implemented through excitatory and inhibitory feedback connections between the two layers. Such a mechanism (either the Gaussian weighting or the refinements over time) would have a more general purpose than just that of decreasing the influence of moving objects. It would also have the effect of sharpening the tuning for the heading estimates. The image velocities near the FOE are the most informative for computing heading (Crowell & Banks, 1993, 1996), so it makes sense to weigh this input more heavily than the less informative input velocities that are further from the FOE. This weighting has the dual result of lessening the effect of noise in the peripheral image velocity vectors

and lessening the effects of moving objects that are not crossing the FOE.

7.2. Alternative neural architectures

The theoretical results presented here suggest that motion subtraction can lead to the biases seen when human subjects judge heading in the presence of moving objects. The results of simulations show that a model using motion-opponent operators to compute these motion differences can account for many of the effects seen with humans. The simulations show that both asymmetric and center-surround spatial arrangements for the receptive fields of these operators yield similar results, suggesting that the results are not dependent on the exact spatial organization of the receptive fields of the operators. Royden (1997) showed that the model's heading responses were also fairly robust to added noise in the velocity field and changes in receptive field size, which suggests that changing these factors would not much change the results presented here. This is reassuring, as the operators used in these simulations are simplified versions of the neurons found in area MT of the primate, which exhibit a variety of receptive field organizations (Xiao et al., 1995). More detailed models of these cells and their inhibitory surrounds will be necessary to ascertain whether they would exhibit the behavior shown in the current simulations.

While the results show that motion-opponent operators can account for most of the human results, there are other neural architectures that could lead to the same effects. Specifically, any neural architecture that leads to a subtraction of velocities from adjacent positions in the visual field will probably exhibit a similar set of results. For example, the inhibition could take place at the level of the connections between the MT neurons and MST cells, with pre-synaptic inhibition taking the place of the motion-opponent receptive field structure simulated here. Another possibility is subtraction at the level of the template layer. For example, Beintema and van den Berg (1998) present a model that makes use of the difference between two templates tuned for opposite directions of rotation when computing heading direction. It seems likely that such a model may also exhibit similar biases to those shown here, although it would be important to verify this by running the appropriate simulations.

7.3. Comparison of model and human results

The motion-opponent model presented here gives results that are very similar to the human results, but they are not identical. This is not surprising because the model uses motion-opponent operators that have simplified versions of the receptive fields of neurons found in MT. Furthermore, the interactions between the components of the model are much simpler than the architecture of the human visual system. It was not our intent to model the MT cells in detail, but rather to show that the motion-opponent receptive field structure could, in principle, account for much of the human data. The overall shape and size of the biases remain similar to that seen with human judgments even with a large change in the receptive field structure between the asymmetric and the center-surround operators, suggesting the basic result is fairly robust. In fact, the average result between these two types of operators fits the human data quite well.

There is one human data point that the model does not fit very well, and that is the leftward bias seen for the object moving in depth with an FOE of 10 deg and starting position of 8.7 deg. The model using asymmetric operators did not show this leftward bias at all. The model using center-surround operators showed a slight leftward bias for this position, but not as large as the human bias. There may be several reasons for this discrepancy. First, the difference could be due to the differences in receptive field structure between the model and actual MT cells. The center-surround structure shows a small leftward bias, and it could be that other variations of this structure would show a bigger bias. Second, both the model and humans have a tendency to report heading closer to the center of the screen as they become more uncertain of the heading. Adding noise to the model input tends to increase the central bias (Royden, 1997), which in this case would be to the left of the simulated headings. It is possible that this condition leads to more uncertainty by the humans than other conditions, causing them to select a more central heading. The final possibility is that this leftward bias is due to some other heading mechanism that operates in addition to or instead of the motion subtraction model suggested here. While the motion subtraction model explains much of the human data, it is possible that this anomalous point will lead us to further insights into the mechanisms of heading perception.

7.4. Comparison with other models

While other models proposed for computing heading could easily add the Gaussian weighting scheme to deal with moving objects, the important property of the Royden (1997) model is that it relies on motion differences which lead to heading biases in the same direction as those seen with human observers. This is not true of template models that use image velocities directly as inputs, such as Hatsopoulos and Warren (1991), or Warren and Saunders (1995). These models give a bias in the direction opposite that seen for laterally moving objects. The Perrone and Stone (1994) model also makes use of image velocities as inputs to templates, and so one would predict that it would also show biases in the

direction opposite object motion for the laterally moving objects, unlike human observers. It would be informative to test this model with these moving object conditions to confirm these predictions. However, the data presented here provide strong support for the idea that velocity differences are important in the mechanism for human heading judgments, since these differences can easily explain the biases seen in human heading judgments. Consequently this lends support to a model such as Royden (1997) or other models that make use of these velocity differences to compute heading.

7.5. Alternative explanations of heading biases

The results presented here suggest that velocity differences can explain the biases in human heading judgments that result from the presence of moving objects in the scene. While this explanation is attractive in that a single theory can explain much of the data, other explanations have been put forward and cannot be ruled out. Several researchers (Pack & Mingolla, 1998; Warren & Saunders, 1995) have suggested that the left and right biases seen with the laterally moving objects (e.g. simulation 1) may be the result of a system to compensate for eye movements. They argue that this lateral bias is similar to an illusory shift of the FOE seen when a plane of laterally moving dots is superimposed on a plane of dots moving in a radial pattern (Duffy & Wurtz, 1993). While it is possible that the results for the laterally moving objects are the result of a mechanism for compensating for eye movements, it seems unlikely, since the observers in the experiments of Royden and Hildreth (1996) were fixating a stationary cross and therefore had a strong non-visual cue that their eyes were not moving. Furthermore, this does not account for the biases seen when the objects are moving in depth, as in simulation 2. These objects present a looming stimulus to the observer, which would likely not stimulate the eye movement compensation mechanism as strongly as the laterally moving objects. While these looming objects do have a component of lateral motion relative to the observer, the bias seen in these conditions is in the direction opposite that predicted by an eye movement compensation model. For example, the object with a 1 deg FOE, starting at a position 5.5 deg to the right of center would have a rightward component of motion relative to the observer. The eye movement compensation theory would predict a rightward bias in this case. However, a leftward bias is seen for human observers. Therefore, to account for the direction of bias seen with objects moving in depth, one must add a second mechanism. For example, Warren and Saunders (1995) suggested that when the FOE of the object is similar to the heading of the observer toward the stationary scene, then the perception is the average of the two. While it is possible that the two effects are the result of separate visual mechanisms, the fact that they can both be explained with a single model using motion differences makes the motion-opponent approach more appealing.

The similarity between the bias seen for laterally moving objects and in the illusion described by Duffy and Wurtz (1993) has been noted several times (Pack & Mingolla, 1998; Warren & Saunders, 1995), and it is likely that they are related. Results from our lab (Royden & Conti, 2002) suggest that a motion-opponent model can also account for the biases seen in the Duffy and Wurtz illusion. The importance of this finding is that one does not have to relate it to eye movements at all, and therefore one does not have to define a separate mechanism for the biases seen with looming objects. Instead, a single explanation can account for multiple effects that result in heading biases. The likely relationship between the Duffy and Wurtz illusion and the biases seen with lateral moving objects suggests that other models that show shifts when presented with the Duffy and Wurtz stimuli may also show biases similar to the Royden model when presented with laterally moving objects. Such models include those of Lappe and Rauschecker (1995) and Beintema and van den Berg (1998). Simulations using these models and appropriate stimuli would test this prediction. It is unclear whether these models would also show the same biases as humans with the looming objects. It would be interesting to run simulations to answer this question.

7.6. Timing of heading judgments

One interesting result in the current study is that the human data fits best with the results of simulations of the stimuli at the beginning of the trials. The model in its current form computes heading from instantaneous velocity information, while human observers have access to information for the entire duration of the trial, which was 0.8 s in Royden and Hildreth (1996). However both the position of the peak heading biases and the magnitude of the biases fit the human data best when computed from velocities early in the trial. One cannot necessarily conclude from this that human observers make their judgments based on information at the beginning of the trial, since it is possible that some parameter changes in the model could lead to other results (although extensive experimentation in this lab has not revealed any such changes). However, it suggests that observers might rely more heavily on the information early in the trial. Beintema and van den Berg (2001), have also found evidence that observers' heading judgments are based primarily on the information present early in the trial. This makes sense for the situation in which the object is moving in depth, because more information from the stationary part of the scene is available at the beginning of each trial than at the end.

The stationary part of the scene is progressively obscured by the image of the object as it expands. Observers can make heading judgments within a 100 ms duration of the stimulus and reach their highest accuracy after about 300 ms (Crowell, Royden, Banks, Swenson, & Sekuler, 1990), so it would be feasible for people to form their judgments from the earliest parts of the trial. While it seems likely that the human estimates result from an integration of information over time, it is possible that the information from the most informative part of the trial, i.e. the beginning, is weighed more heavily.

8. Conclusion

In conclusion, the data presented here show that a model based on motion-opponent properties of cells in MT can account for most of the biases seen in human heading judgments in the presence of moving objects. This is an important finding, since it can explain the seemingly contradictory results from the human psychophysics, in which lateral object motion leads to judgment biases in the direction of the object motion, while object motion in depth leads to biases in the direction opposite the lateral component of object motion. It should be stressed that the model tested here was developed to describe how humans might judge their heading in the presence of rotations, assuming motion through a stationary scene. It is remarkable that, when applied to the novel situation of a scene containing moving objects, the model performs so similarly to humans. This lends support to the idea that the human mechanism for computing heading makes use of motion differences. Although there are a variety of mechanisms by which these differences may be computed, the fact that many MT cells have receptive field structures that could compute these velocity differences makes these cells likely candidates for the initial stage of computing heading.

Acknowledgements

This work was supported by NSF grant #IBN-0196068. The author thanks Ellen Hildreth for helpful comments on the manuscript and Timothy Hattori, Laura Picone and Nora Newman for help with the collection and analysis of the data.

References

Allman, J., Miezin, F., & McGuiness, E. (1985). Direction- and velocity-specific responses from beyond the classical receptive field in the middle temporal visual area (MT). *Perception, 14*, 105–126.

Bruss, A. R., & Horn, B. K. P. (1983). Passive navigation. *Computer Vision, Graphics, and Image Processing, 21*, 3–20.

Beintema, J. A., & van den Berg, A. V. (1998). Heading detection using motion templates and eye velocity gain fields. *Vision Research, 38*, 2155–2179.

Beintema, J. A., & van den Berg, A. V. (2001). Pursuit affects precision of perceived heading for small viewing apertures. *Vision Research, 41*, 2375–2391.

Cutting, J. E., Springer, K., Braren, P. A., & Johnson, S. H. (1992). Wayfinding on foot from information in retinal, not optical, flow. *Journal of Experimental Psychology: General, 121*, 41–72.

Cutting, J. E., Vishton, P. M., & Braren, P. A. (1995). How we avoid collisions with stationary and moving objects. *Psychological Review, 102*, 627–651.

Crowell, J. A., & Banks, M. S. (1993). Perceiving heading with different retinal regions and types of optic flow. *Perception and Psychophysics, 53*, 325–337.

Crowell, J. A., & Banks, M. S. (1996). Ideal observer for heading judgments. *Vision Research, 36*, 471–490.

Crowell, J. A., Royden, C. S., Banks, M. S., Swenson, K. H., & Sekuler, A. B. (1990). Optic flow and heading judgments. *Investigative Ophthalmology and Visual Science, 31*(Suppl.), 522.

Duffy, C. J., & Wurtz, R. H. (1991). Sensitivity of MST neurons to optic flow stimuli. I. A continuum of response selectivity to large field stimuli. *Journal of Neurophysiology, 65*, 1329–1345.

Duffy, C. J., & Wurtz, R. H. (1993). An illusory transformation of optic flow fields. *Vision Research, 33*, 1481–1490.

Duffy, C. J., & Wurtz, R. H. (1995). Response of Monkey MST neurons to optic flow stimuli with shifted centers of motion. *Journal of Neuroscience, 15*, 5192–5208.

Gibson, J. J. (1950). *The perception of the visual world*. Boston, Mass: Houghton Mifflin.

Graziano, M. S. A., Andersen, R. A., & Snowden, R. (1994). Tuning of MST neurons to spiral motions. *Journal of Neuroscience, 14*, 54–67.

Hatsopoulos, N. G., & Warren, W. H. (1991). Visual navigation with a neural network. *Neural Networks, 4*, 303–317.

Heeger, D. J., & Jepson, A. D. (1992). Subspace methods for recovering rigid motion I: Algorithm and implementation. *International Journal of Computer Vision, 7*, 95–117.

Hildreth, E. C. (1992). Recovering heading for visually-guided navigation. *Vision Research, 32*, 1177–1192.

Lappe, M., & Rauschecker, J. P. (1993). A neural network for the processing of optic flow from ego-motion in man and higher mammals. *Neural Computation, 5*, 374–391.

Lappe, M., & Rauschecker, J. P. (1995). An illusory transformation in a model of optic flow processing. *Vision Research, 35*, 1619–1631.

Longuet-Higgins, H. C., & Prazdny, K. (1980). The interpretation of a moving retinal image. *Proceedings of the Royal Society of London B, 208*, 385–397.

Maunsell, J. H. R., & van Essen, D. C. (1983). Functional properties of neurons in middle temporal visual area of the macaque monkey. I. Selectivity for stimulus direction, speed and orientation. *Journal of Neurophysiology, 49*, 1127–1147.

Pack, C., & Mingolla, E. (1998). Global induced motion and visual stability in an optic flow illusion. *Vision Research, 38*, 3083–3093.

Perrone, J. A. (1992). Model for the computation of self-motion in biological systems. *Journal of the Optical Society of America, A, 9*, 177–194.

Perrone, J. A., & Stone, L. S. (1994). A model of self-motion estimation within primate extrastriate visual cortex. *Vision Research, 34*, 2917–2938.

Raiguel, S., Van Hulle, M. M., Xiao, D. K., Marcar, V. L., & Orban, G. A. (1995). Shape and spatial distribution of receptive fields and antagonistic motion surrounds in the middle temporal area (V5) of the macaque. *European Journal of Neuroscience, 7*, 2064–2082.

Rieger, J. H., & Lawton, D. T. (1985). Processing differential image motion. *Journal of the Optical Society of America A, 2*, 354–360.

Royden, C. S. (1997). Mathematical analysis of motion-opponent mechanisms used in the determination of heading and depth. *Journal of the Optical Society of America A, 14*, 2128–2143.

Royden, C.S., & Conti, D. (2002). A model using velocity differences to compute heading can explain an illusory transformation of optic flow fields. *Vision Sciences Society Annual Meeting Abstract*, Sarasota Florida.

Royden, C. S., & Hildreth, E. C. (1996). Human heading judgments in the presence of moving objects. *Perception and Psychophysics, 58*, 836–856.

Saito, H., Yukie, M., Tanaka, K., Hikosaka, K., Fukada, Y., & Iwai, E. (1986). Integration of direction signals of image motion in the superior temporal sulcus of the macaque monkey. *Journal of Neuroscience, 6*, 145–157.

Tanaka, K., & Saito, H. (1989). Analysis of motion in the visual field by direction, expansion/contraction, and rotation cells clustered in the dorsal part of the medial superior temporal area of the macaque monkey. *Journal of Neurophysiology, 62*, 626–641.

Warren, W. H., & Saunders, J. A. (1995). Perceiving heading in the presence of moving objects. *Perception, 24*, 315–331.

Xiao, D. K., Raiguel, S., Marcar, V., Koenderink, J., & Orban, G. A. (1995). Spatial heterogeneity of inhibitory surrounds in the middle temporal visual area. *Proceedings of the National Academy of Science USA, 92*, 11303–11306.